Vortex dynamics in incompressible Richtmyer-Meshkov instability with surface tension

Chihiro Matsuoka*
Department of Physics,
Graduate School of Science and Technology,
Ehime University, Matsuyama, Ehime 790-8577, Japan

Abstract

Motion of a planar interface in incompressible Richtmyer-Meshkov (RM) instability with surface tension is investigated numerically by use of the boundary integral method. It is shown that an interface rolls up without regularization of the interfacial velocity when the Atwood number is relatively small. The comparison between the growth rate of an interface with and without surface tension is made, and we present that the growth rate of the interface with surface tension is equal to the one without surface tension at the asymptotic stage when the Atwood number is identical to each other. A phenomenon known as 'pinching' in the physics of drops is found in the final stage of calculations for relatively small Atwood numbers and it is shown that this phenomenon is caused by a vortex pair induced on the interface. We also present that when the surface tension coefficient is relatively large, stable oscillatory motion appears for RM instability. When the gravity is taken into account, linearly stable but asymptotically unstable motion can appear under a certain condition of three parameters; the Atwood number, the gravity and the surface tension.

1 INTRODUCTION

When an inhomogeneous vorticity initially distributes on an interface between two fluids with different densities and it is driven by some external force such as a shock wave, a corrugated interface eventually rolls up to a mushroom-like structure. This phenomenon, known as the Richtmyer-Meshkov (RM) instability [1, 2], is important in various areas such as astrophysical supernova [4], supersonic combustion and the inertial confinement fusion. Due to the existence of density inhomogeneity in the system, the RM instability can be also a model of an inhomogeneous and nonuniform turbulence, together with the Rayleigh-Taylor (RT) instability [3].

When the surface tension effect exists on the interface, the RM and RT instabilities can describe the pure capillary wave and capillary-gravity wave [5, 6], respectively in the limit of Atwood number $A = 1$ (see Sec. 2 for the definition of A). These describe relatively low velocity flow without vortex motion, i.e., shear velocity motion, however, there exists high velocity motion with surface tension such as breakup of drops in two-fluid ($A \neq 0$) inviscid systems [7]. One of such systems is the impact of meteorites on the primitive earth [8], in which meteorites in liquid state collide on the surface of

---

*matsuoka@phys.sci.ehime-u.ac.jp

the earth at high speed. This is an example of motion of an unstable fluid interface with density stratification and surface tension. It seems that the surface tension effect is considerably small in some real experiments for the RM instability, for instance, such that the interfacial instability is generated by impulsively accelerating a tank containing two liquids reported by Jacobs et al. [9]-[11], however, that can be important when the liquids used in experiments are replaced another ones in which the surface tension effect cannot disregard.

As is well-known, the surface tension term is expressed by the derivative of curvature of the interface, therefore, it contains the highest spatial derivative in the governing equations (see Sec. 2) and this term governs interfacial motion in the high wave numbers together with the convective term which gives rise to vortex motion. When the surface tension term is sufficiently large, the effect may suppress the vortex motion such as the roll-up of the interface [12, 13]. Hou et al. [14, 15] numerically examined the long-time motion of vortex sheet with surface tension for the density matched $(A = 0)$ case and observed a phenomenon called 'pinching singularity' in the physics of drops [7].

Pinching or pinch-off is a phenomenon observed in capillary-driven motion of free surface flows when the convective nonlinearity, i.e., vortex motion is taking into account in the system [7, 16]. The pinching phenomenon is important for the process which a single drop breaks up into several drops and the pinching singularity or pinch-off is observed as a phenomenon at which the interfacial curvature and the interfacial velocity diverge to infinity. This singularity is peculiar to surface tension driven motion and it is considered [14, 15, 16, 20] as different from Moore's curvature singularity [17] which is observed in the inviscid vortex motion without surface tension. Hou et al. [14, 15, 20] calculated this pinching singularity with high accurate numerical scheme and obtained a result that the pinching region does not perfectly stick and there exists a narrow gap. This pinching singularity is hard to appear for larger Atwood numbers (see Secs. 3 and 4).

In this article we examine the effect that the surface tension gives to the interfacial motion in the RM instability and show the results which do not appear in the zero surface tension case [12, 13, 18, 19] or in the density matched case [14, 15]. The well-known result that the linear growth rate in the RM instability is proportional to time t does not hold for finite surface tension case. This result, which can be easily expected from the linear stability analysis, is also confirmed in our numerical calculations. As the surface tension parameter becomes large, the roll-up of the interface disappears and a stable oscillatory motion appears instead. The frequency of this oscillation depends on the surface tension parameter for a fixed Atwood number and the motion is not so regular as the standing wave motion for the RT instability [20].

When the gravity is taking into account, i.e., for the RT instability, linearly stable but asymptotically unstable motion appears when three parameters, the Atwood number, the gravity and the surface tension coefficient satisfy a certain condition. This corresponds to a critical or marginally stable state at which the system changes from stable to unstable. The existence of such critical motion can be also expected from the linear stability analysis, however, it has never presented how the motion is. We show that a kind of pinching phenomenon appears at the final stage of this critical motion (see Sec. 4.3). In Sec. 2 we present governing equations which are used for our numerical calculations. In Sec. 3 we present interfacial motion for the RM instability with various Atwood numbers and surface tension parameters using the scheme presented by Hou et al. [14]. Stable oscillatory motion in the RM instability and motion taking into account the gravity, i.e., motion in the RT instability are presented in Sec. 4. Section 5 is devoted to discussions and conclusion.

2 GOVERNING EQUATIONS

We consider a two-dimensional system, therefore, the interface is assumed to be a curve between two fluids with different densities. The governing equations are equations which describes the interfacial position (x, y) and the pressure boundary condition, i.e., the Laplace-Young condition. Due to the strong numerical instability caused by the surface tension term, the long-time computation is impossible with the explicit method which we have used for the vortex sheet motion with zero surface tension parameter [13)18)-19)]. Instead, we adopt here the formulation which was presented by Hou *et al.* [14)] in order to calculate the interfacial motion with surface tension. We briefly review the method here for convenience and completeness.

2.1 The formulation for numerical calculations

The temporal evolution of the interface $\boldsymbol{X} = (x(\beta, t), y(\beta, t))$ is given by

$$\boldsymbol{X}_t = U\boldsymbol{n} + T\boldsymbol{t}, \tag{1}$$

where β is a Lagrangian parameter which parameterize the interface, t is time, U and T are the normal and tangential velocities of the interface, respectively, and the subscript denotes the differentiation with respect to the variable. The unit normal $\boldsymbol{n}$ and the unit tangent $\boldsymbol{t}$ are described by the tangent angle θ to the interface as

$$\boldsymbol{n} = (-\sin\theta, \cos\theta), \quad \boldsymbol{t} = (\cos\theta, \sin\theta).$$

By Frenet's formula for plane curves, we have

$$\boldsymbol{t}_s = K\boldsymbol{n}, \quad \boldsymbol{n}_s = -K\boldsymbol{t},$$

where K is curvature of the interface and s is arc length given by $s = \int \sqrt{x_\beta^2 + y_\beta^2} d\beta$. The interfacial position is specified with s_β and θ as follows:

$$s_{\beta,t} = T_\beta - \frac{\theta_\beta^2}{s_\beta}, \tag{2a}$$

$$\theta_t = \frac{1}{s_\beta}\left(\frac{\theta_\beta}{s_\beta}\right)_\beta + \frac{T}{s_\beta}\theta_\beta. \tag{2b}$$

We assume that the flow is incompressible and inviscid. Then the pressure boundary condition, i.e., the Laplace-Young condition which holds at the interface

$$p_1 - p_2 = \sigma K, \tag{3}$$

is rewritten into the form

$$\rho_1\left[\frac{\partial\phi_1}{\partial t} + \frac{1}{2}\left(\nabla\phi_1\right)^2 + g\right] - \rho_2\left[\frac{\partial\phi_2}{\partial t} + \frac{1}{2}\left(\nabla\phi_2\right)^2 + g\right] = \sigma K, \tag{4}$$

where ρ_i is the density of fluid i ($i = 1, 2$), p_i is the pressure in fluid i, g is the gravity, σ is the surface tension coefficient and ϕ_i is the velocity potential in fluid i which is related to each fluid velocity $\boldsymbol{u}_i$ as $\boldsymbol{u}_i = \nabla\phi_i$. Note that $\triangle\phi_i = 0$ holds in each fluid region by the incompressibility condition.

Differentiating Eq. (4) with respect to β, we obtain the following Fredholm integral equation of the second kind:

$$\gamma_t = \sigma K_\beta + \left(\frac{T^A \gamma}{s_\beta}\right)_\beta + 2A\left[s_\beta \boldsymbol{W}_t \cdot \boldsymbol{t} + \frac{1}{8}\left(\frac{\gamma}{s_\beta}\right)^2_\beta - T^A \boldsymbol{W}_\beta \cdot \boldsymbol{t} + g y_\beta\right], \tag{5}$$

where γ is related with the circulation $\Gamma \equiv \phi_1 - \phi_2$ as $\gamma = \Gamma_\beta$, the Atwood number A is given by $A = (\rho_2 - \rho_1)/(\rho_1 + \rho_2)$ and we normalize the surface tension coefficient $\sigma \rightarrow 2\sigma/(\rho_1 + \rho_2)$. The velocity $\boldsymbol{W} = (W_x, W_y)$ induced by the vortex sheet is given by the Birkhoff-Rott equation [21]

$$
\begin{aligned}
W_x &= \operatorname{Re}\left[\frac{1}{2\pi i}\text{P.V.}\int_{-\infty}^{\infty}\frac{\gamma(\beta',t)d\beta'}{Z(\beta,t) - Z(\beta',t)}\right], \\
W_y &= -\operatorname{Im}\left[\frac{1}{2\pi i}\text{P.V.}\int_{-\infty}^{\infty}\frac{\gamma(\beta',t)d\beta'}{Z(\beta,t) - Z(\beta',t)}\right],
\end{aligned}
\tag{6}
$$

where P.V. denotes the principal value and $Z = x + iy$. The tangential velocity T is decomposed into the form

$$T = T^A + \boldsymbol{W} \cdot \boldsymbol{t}, \tag{7}$$

where T^A is an arbitrary tangential velocity and its choice determines the frame of reference. The normal velocity U is given by $U = \boldsymbol{W} \cdot \boldsymbol{n}$ in our formulations.

The arbitrary tangential velocity T^A cannot take the same form between $\sigma = 0$ and $\sigma \neq 0$. When the surface tension coefficient $\sigma = 0$, the arbitrary tangential velocity T^A is chosen as [13, 18, 19, 22]

$$T^A = \frac{\alpha}{2s_\beta}\gamma, \tag{8}$$

in our calculations, where $\alpha = \alpha(A)$ is an artificial parameter such that $\alpha \neq 0$ for $A \neq 0$. When $\sigma \neq 0$, the arbitrary tangential velocity T^A is chosen as

$$T^A = \boldsymbol{W} \cdot \boldsymbol{t} + \int_0^\beta \left(\theta_\beta U - \frac{1}{2\pi}\int_0^{2\pi}\theta'_\beta U d\beta'\right) d\beta, \tag{9}$$

in which $s_\beta = \frac{1}{2\pi}\int_0^{2\pi} s'_\beta d\beta'$ is set to be everywhere equal to its mean [14, 15], i.e., s_β is a constant with respect to β for a fixed time t.

By solving Eqs. (2a), (2b) and (5), we can recover (x, y, κ) from $(s_\beta, \theta, \gamma)$ using the relation

$$
\begin{aligned}
x &= \int_0^\beta s'_\beta \cos\theta(\beta')d\beta' + \beta, \\
y &= \int_0^\beta s'_\beta \sin\theta(\beta')d\beta',
\end{aligned}
\tag{10}
$$

where $\kappa = \gamma/s_\beta$ is the true vortex sheet strength which is frame independent.

2.2 Spatial discretization and numerical scheme

As we stated in Sec. 1, K_β in Eq. (5) causes strong numerical instability called 'stiffness'. In order to avoid this instability, we decompose the Cauchy integral in Eq. (6) as

$$
\begin{aligned}
\text{P.V.}\int_{-\infty}^{\infty}\frac{\gamma(\beta',t)d\beta'}{Z(\beta,t) - Z(\beta',t)} = \text{P.V.}\int_{-\infty}^{\infty}&\left[\frac{1}{Z_\beta(\beta - \beta')}\right. \\
+ &\left.\left(\frac{1}{Z(\beta,t) - Z(\beta',t)} - \frac{1}{Z_\beta(\beta - \beta')}\right)\right]\gamma(\beta',t)d\beta'.
\end{aligned}
\tag{11}
$$

Then the normal velocity can be expressed as

$$U(\beta, t) = \frac{1}{2s_\beta} H[\gamma](\beta, t) + E[\gamma](\beta, t), \tag{12}$$

where $H[\gamma]$ is the Hilbert transform of γ and the Fourier component of $E[\gamma]$ is exponential decay for high mode [23].

Expanding (θ, γ) with Fourier modes

$$\theta = \sum_{n=-\frac{N}{2}+1}^{\frac{N}{2}} \hat{\theta}_n e^{in\beta}, \quad \gamma = \sum_{n=-\frac{N}{2}+1}^{\frac{N}{2}} \hat{\gamma}_n e^{in\beta},$$

and substituting these into Eqs. (2b) and (5), we have

$$\begin{aligned}
\hat{\theta}_t &= \frac{|n|}{2s_\beta^2} \hat{\gamma}(n) + \hat{P}(n), \\
\hat{\gamma}_t &= -\frac{\sigma n^2}{s_\beta} \hat{\theta}(n) + \hat{Q}(n),
\end{aligned} \tag{13}$$

where N is the grid number, i.e., the number of point vortices, and $\hat{P}(n)$ and $\hat{Q}(n)$ are Fourier transformed remainder terms in the original equations Eqs. (2b) and (5), respectively. The equation for s_β in Eq. (2a) is solved without applying the Fourier transform.

Following Hou et al. [14], we use the second order Adams-Bashforth method and the Crank-Nicholson scheme in order to perform the temporal integration for s_β in Eqs. (2a) and (13), respectively. Applying these explicit and implicit method simultaneously, we can recover s_β, θ and γ, therefore, x, y and κ using the inverse Fourier transform after each temporal integration. The spatial integrations of the first and the second terms on the right hand side of Eq. (11) are calculated with the alternate point quadrature method [24] and the trapezoidal rule, respectively. There also exists explicit stable numerical method with spectral accuracy [25], however, calculations with that method break down before appearing the pinching singularity.

3   Pinching phenomenon in Richtmyer-Meshkov instability

In this section we show some numerical results for motion of the interface in the RM instability with surface tension. For those calculations, we normalize $\beta \to k\beta$, $x \to kx$, $y \to ky$ and $t \to kv_{lin}t$ [12, 13] with the asymptotic linear growth rate v_{lin} [26] and the wave number k in the system. When $\sigma \neq 0$, we adopt the implicit scheme stated in Sec. 2.2, while we use the explicit scheme (the fourth order Runge-Kutta scheme) which was adopted in Ref. [13] when $\sigma = 0$. For the former case, the arbitrary tangential velocity T^A is chosen in the form of Eq. (9), while T^A is chosen in the form of Eq. (8) for the latter case. All calculations throughout this paper except the calculation for $\sigma = 0$ in Fig. 4 (see Sec. 3.1) are performed without regularization [27] of the Cauchy integral in Eq. (6).

Initial conditions for all calculations in the RM instability are taken that

$$x(\beta, 0) = \beta, \quad y(\beta, 0) = 0, \quad \gamma(\beta, 0) = 2\sin\beta, \tag{14}$$

for both of $\sigma = 0$ and $\sigma \neq 0$, and we set $g = 0$ in Eq. (5) for the RM instability. The periodic boundary condition is imposed and the interval $[-\pi, \pi]$ is basically divided with grid number $N = 1024$. For calculations such that the pinching singularity appears, we refine the grid number N from $N = 1024$ to $N = 2048$. We set the upper fluid (ρ_2, $y > 0$) is heavier than the lower fluid (ρ_1, $y < 0$) for all calculations including the RT instability (see Sec. 4).
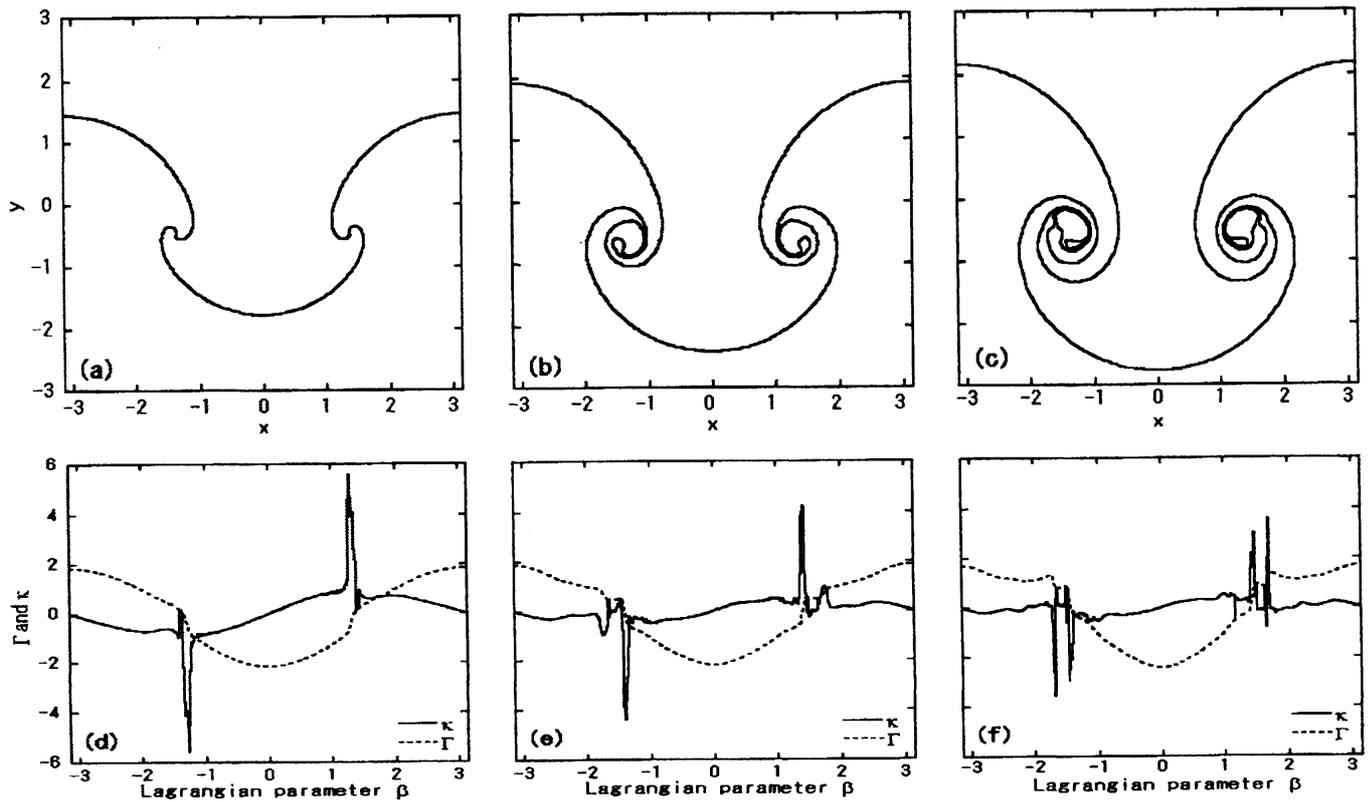
Fig. 1: Interfacial profiles, circulation Γ and sheet strength κ for $A = 0.2$ and $\sigma = 0$ at $t = $ (a) and (d) 2.6, (b) and (e) 5.0, and (c) and (f) 6.2, where dashed and solid lines in (d) – (f) denote the circulation Γ and the sheet strength κ, respectively. The regularized parameter δ is set to $\delta = 0.1$ here.
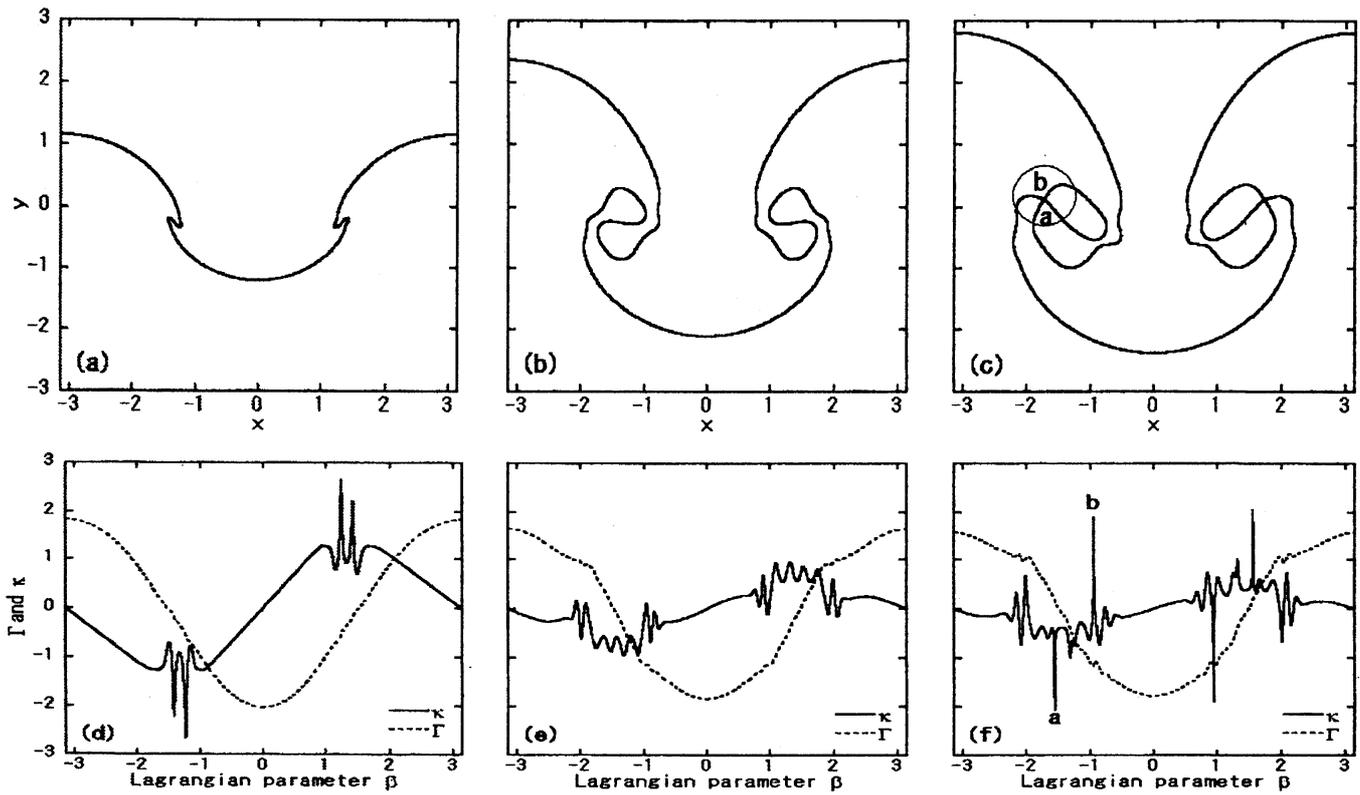
Fig. 2: Interfacial profiles, circulation Γ and sheet strength κ for $A = 0.2$ and $\sigma = 0.05$ at $t =$ (a) and (d) 1.5, (b) and (e) 5.0, and (c) and (f) 7.15, where dashed and solid lines in (d) $-$ (f) denote the circulation Γ and the sheet strength κ, respectively. The circled region in (c) is magnified in Fig. 3.

3.1 Pinching singularity with small surface tension coefficient

We show interfacial profiles in 1 (a) - (c) for the Atwood number $A = 0.2$ and the surface tension coefficient $\sigma = 0$, where (d) - (f) show the circulation $\Gamma = \int \gamma d\beta$ and the true vortex sheet strength $\kappa = \gamma/s_\beta$ at the corresponding time. The time step Δt for the temporal integration and the grid number N are set to $\Delta t = 1.25 \times 10^{-4}$ and $N = 1024$, respectively. Time $t = 6.2$ is the breakdown time just after which the computation breaks down. We set here Krasny's regularized parameter $delta = 0.1$ [13, 27], and the arbitrary tangential velocity T^A is chosen in the form of Eq. (8). The roll-up for $\sigma = 0$ is tighter than the one for finite σ and the peak values of the sheet strength κ are larger than those for finite σ (see Fig. 2), i.e., the interface for $\sigma = 0$. We see that the circulation Γ is relatively smooth even though just before the break-down. For the temporal evolution of the interface with another Atwood number, refer to the reference 13).
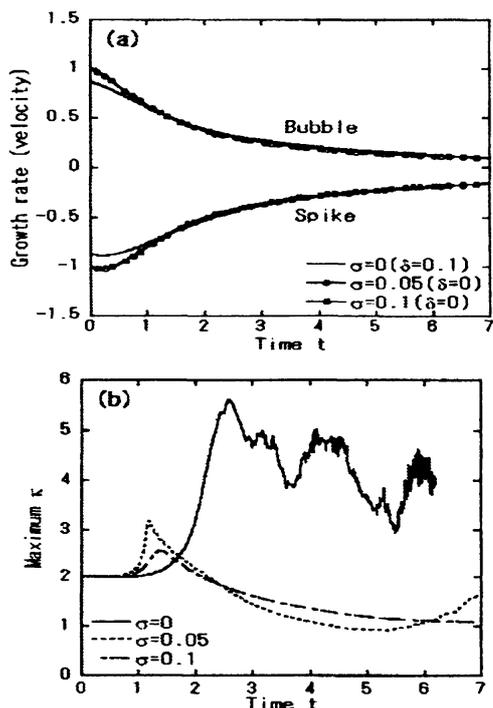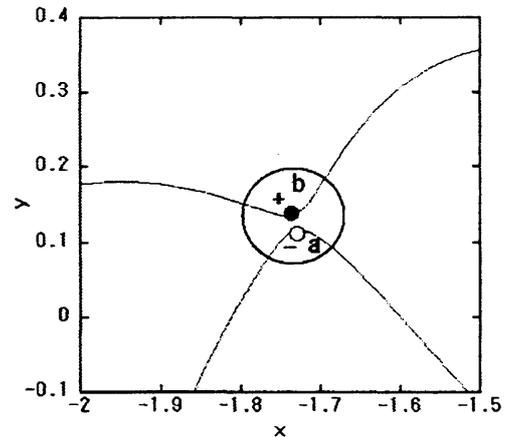

Fig. 3: Magnified figure of circled region in Fig. 2 (c).

Figure 2 (a) - (c) show interfacial profiles, while (d) - (f) show the circulation Γ and the true vortex sheet strength κ at the corresponding time for the Atwood number $A = 0.2$ and the surface tension coefficient $\sigma = 0.05$. The time step Δt for the temporal integration is set to $\Delta t = 1.25 \times 10^{-4}$ and the grid number N is refined from $N = 1024$ ($0 \leq t \leq 6.0$) to $N = 2048$ ($6.0 \leq t \leq 7.15$). After a few time steps from $t = 7.15$, the computation breaks down. The interface rolls up without regularization of the Cauchy integral in equation (6), i.e., without the use of Krasny's δ, although the roll-up is looser in comparison with the case of $\sigma = 0$ [13]. The maximum (peak) value, i.e., the core strength [13] in the sheet strength κ at $t = 1.5$ is larger than the one at $t = 7.15$, however, more Fourier modes are created in κ and concentration of peak values becomes stronger at $t = 7.15$. This tendency is also found in κ for $\sigma = 0$ (see Fig. 1).

The magnified figure of the circled region in Fig. 2 (c) is shown in Fig. 3. This part (and the symmetric part with respect to the y-axis) is called 'pinch-off' or 'pinching singularity' region [7, 14, 15, 16]. As we see from this figure, the pinching region does not stick perfectly and there is a narrow gap between closest two points. Before these two points stick perfectly, the calculation breaks down if the accuracy of the calculation is sufficiently good. This gap becomes wider as the Atwood number be-

Fig. 4: Growth rate (velocity) of bubble and spike (a) and the absolute value of maximum sheet strength (core strength) κ (b) for $A = 0.2$, where the regularized parameter δ is chosen that $\delta = 0.1$ for $\sigma = 0$. The computation for $\sigma = 0$ breaks down at $t = 6.2$.

comes large. When the Atwood number $A = 0$, the pinching singularity appear at four points [see Fig. 6 (a)].

Pinching is caused due to a vortex pair which exists at the tip of the closest two points. We show strong vorticity with plus (b) and minus (a) sign with black and white circle, respectively in the figure, where the corresponding peaks in κ are shown in Fig. 2 (f). This vortex pair has slightly minus net vorticity and the other vortex pair which is in the symmetrical position with respect to the y-axis has slightly plus net vorticity. Pinching singularity is a phenomenon which is caused due to the competition between the inertial force and the surface tension, and it is not observed for a vortex sheet with $\sigma = 0$, i.e., this singularity is different from the well-known Moore's curvature singularity [17] [see Fig.5 (a) and (d)]. When the surface tension coefficient is large, pinching in the RM instability does not appear even though the Atwood number is small.

We show the growth rate, i.e., the velocity of bubble and spike for $\sigma = 0$, $\sigma = 0.05$ and $\sigma = 0.1$ with the same Atwood number $A = 0.2$ in Fig. 4 (a). When $\sigma = 0$, there exists deviation from ± 1 which is the exact value of the growth rate of bubble and spike at $t = 0$. This deviation is caused by the existence of the finite regularized parameter δ [18], where we set to $\delta = 0.1$ for the calculation of $\sigma = 0$. When we set to $\delta = 0$, this deviation disappears (see Fig. 7), however, the breakdown of computation arises at earlier time [see Fig. 5 (a) and (d)]. We see that the asymptotic growth rate of bubble and spike coincides for three σ when we fix an Atwood number. This tendency is unchanged even though we choose another value of δ for $\sigma = 0$ or larger σ for calculations of $\sigma \neq 0$ as long as the Atwood number is not close to 1. Figure 4 (b) shows the absolute value of maximum sheet strength (peak value) κ for the corresponding parameters with (a). The maximum sheet strength for $\sigma = 0$ has the largest value in all σ and the value becomes smaller as the surface tension coefficient σ becomes large. This tendency is also true for another Atwood numbers.

3.2 Interfacial profiles for various Atwood numbers and surface tension coefficients

Figure 5 show interfacial and curvature profiles for a fixed Atwood number $A = 0.2$ and various σ with the regularized parameter $\delta = 0$. The time step is taken that $\Delta t = 1.25 \times 10^{-5}$ for $\sigma = 0$ calculation, while $\Delta t = 1.25 \times 10^{-4}$ for $\sigma = 0.1$ and 0.3 calculations. The profiles for $\sigma = 0$ and $\sigma = 0.1$ are the ones at just before their breakdown times, where the refinement from $N = 1024$ ($0 \leq t \leq 8.0$) to $N = 2048$ ($8.0 \leq t \leq 9.0$) is performed for the calculation of $\sigma = 0.1$. We see that the interfacial profile (a) is smooth and the amplitude of it is small, however, the curvature (d) is very large. This is well-known Moore's curvature singularity [17] for $\delta = 0$ and $\sigma = 0$. Note that the interface for $\sigma = 0$ does not roll up unlike the case for finite δ. The circled region in (b) does not stick perfectly as found in Fig. 3, where sharp peaks in the curvature profile (e) correspond to closest two points in that region. When the surface tension coefficient σ is large ($\sigma \geq 0.2$), both of the curvature and the peak values in the sheet strength κ are small, and the circulation Γ almost does not change its shape from the initial state. The pinching phenomenon was not found for $\sigma \geq 0.2$ with all Atwood numbers. The calculation for $\sigma = 0.3$ is stable and the breakdown of computation does not occur even at past $t = 15$ (see Sec. 4.2).

Figure 6 shows interfacial profiles for various Atwood numbers with a fixed surface tension coefficient $\sigma = 0.05$. Time denoted in each figure caption corresponds to just before time at which the calculation breaks down, where the time step is taken that $\Delta t = 1.25 \times 10^{-4}$ for all calculations. A refinement from $N = 1024$ to $N = 2048$ is performed for $A = 0$ and $A = 0.5$ calculations, where the former grid number is taken over $0 \leq t \leq 4.0$ for $A = 0$ and $0 \leq t \leq 10.0$ for $A = 0.5$, while the latter grid number is taken over $4.0 \leq t \leq 4.9$ for $A = 0$ and $10.0 \leq t \leq 11.5$ for $A = 0.5$, respectively. When $A = 0$, the pinching singularity appear at four points (circled
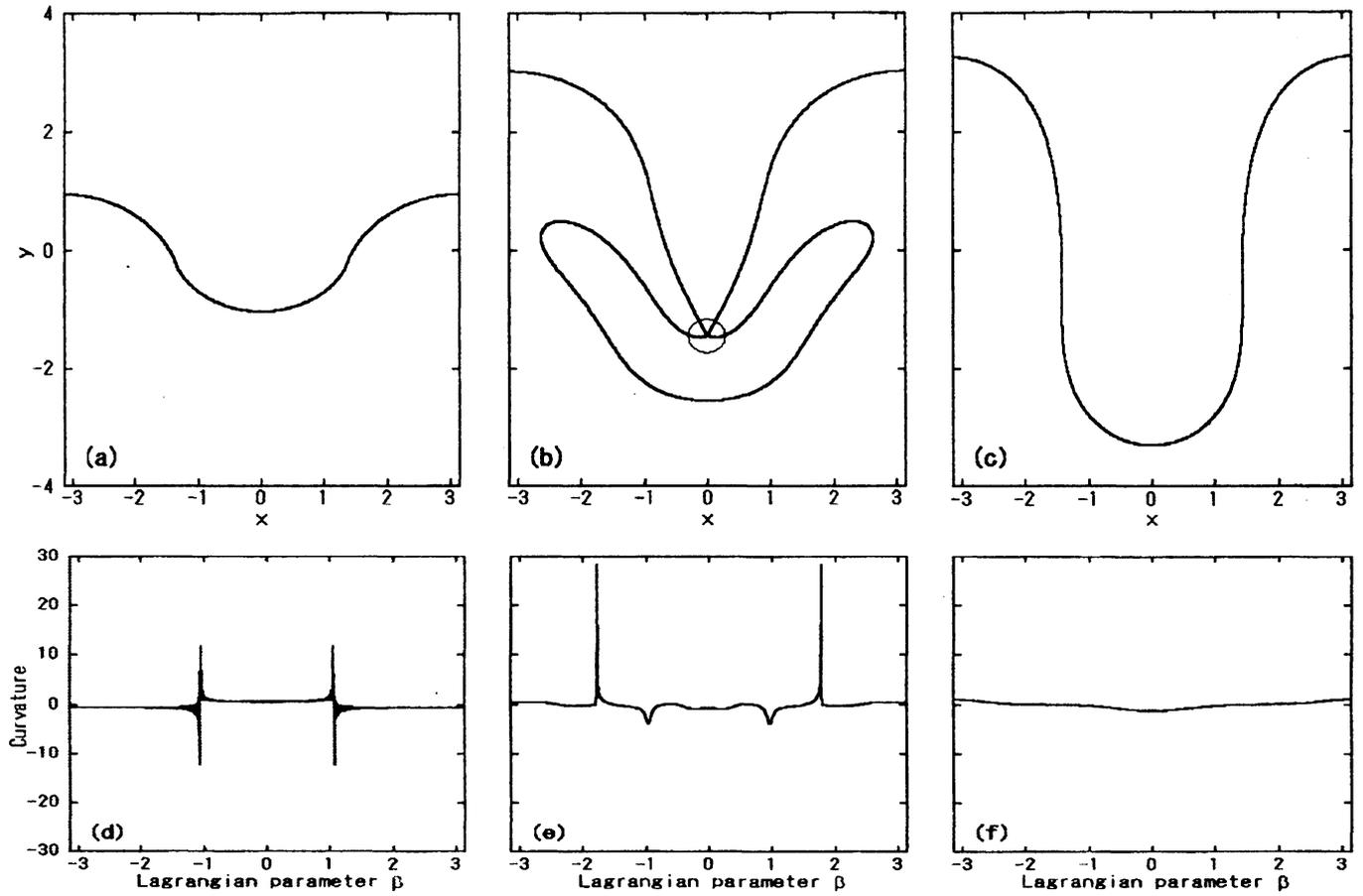
Fig. 5: Interfacial profiles for $A = 0.2$ with various σ; (a) $\sigma = 0$ and $t = 0.93$, (b) $\sigma = 0.1$ and $t = 9.0$, and (c) $\sigma = 0.3$ and $t = 12.0$, where (d) $-$ (f) are curvature profiles corresponding to (a) $-$ (c), respectively. The regularized parameter δ is set to $\delta = 0$ for all calculations.
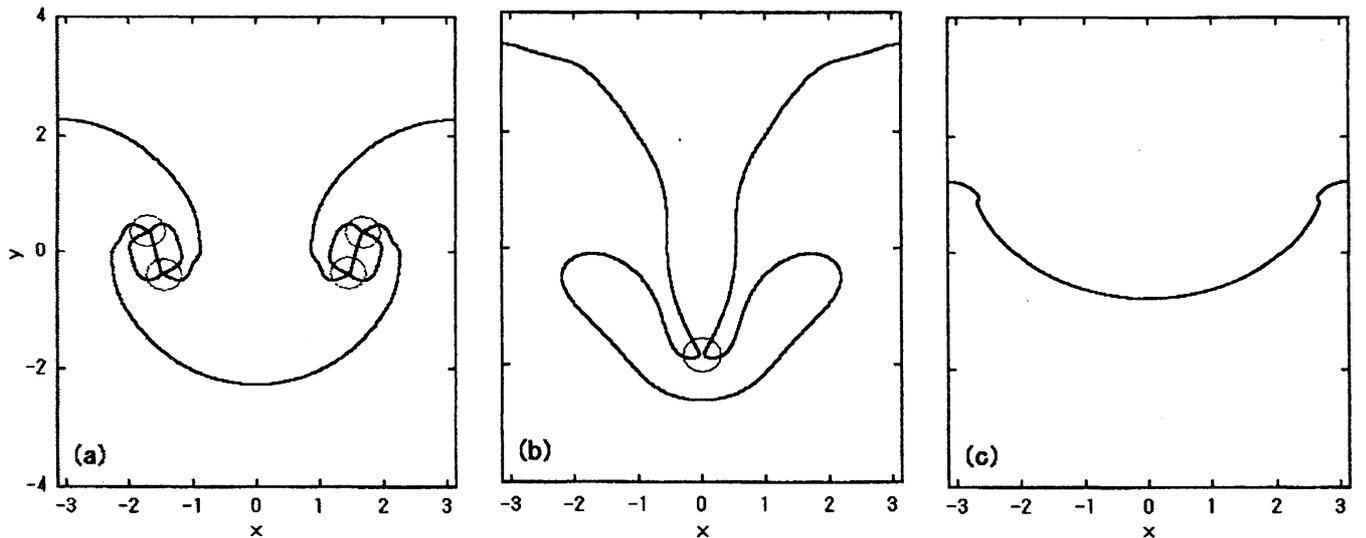

Fig. 6: Interfacial profiles for various Atwood numbers; (a) $A = 0$ and $t = 4.9$, (b) $A = 0.5$ and $t = 11.5$, and (c) $A = 1.0$ and $t = 1.1$, where $\sigma = 0.05$ for all calculations. The circled regions in (a) and (b) do not stick perfectly.

regions in (a)). The closest two points of the interface do not stick perfectly at all pinching points as found in Fig. 3, however, the gap between two points is narrower than that for $A = 0.2$. The profile (b) for $A = 0.5$ is similar to the one in Fig. 5 (b), however, the gap between the closest two points of the circled region is wider than the gap for $A = 0.2$.

4 Linear stability, stable oscillatory motion in Richtmyer-Meshkov instability and unstable motion in Raighley-Taylor instability

4.1 Linear stability analysis

When the surface tension coefficient becomes still larger, motion of the interface becomes stable. Linear stability analysis suggests this fact. The linear growth rate of this system is calculated by equation (4) and the kinematic boundary condition

$$\frac{\partial \eta}{\partial t} + \frac{\partial \phi_i}{\partial x}\frac{\partial \eta}{\partial x} = \frac{\partial \phi_i}{\partial y}, \quad (i = 1, 2) \tag{15}$$

where $y = \eta(x, t)$ is the deviation of the interface. Within the linear approximation, the deviation η is given as

$$\eta \propto e^{i(\omega t - x)}, \tag{16}$$

in our normalization, in which

$$\omega = \sqrt{\frac{\sigma}{2} - Ag}, \tag{17}$$

[if we do not normalize the length with wave number k, Eq. (16) and Eq. (17) are given as $\eta \propto e^{i(\omega t - kx)}$ and $\omega = (\sigma k^3/2 - Agk)^{1/2}$, respectively].

Equation (16) indicates that when the surface tension exists, the well-known linear growth rate in the RM instability ($g = 0$) which is proportional to time t [1, 12, 26] does not hold any longer and motion is stable within the linear stability analysis. When the surface tension is finite but sufficiently small, the inertial force which produces the vorticity and governs the nonlinear stage is more effective in the system, therefore, the linear solution (16) does not affect in the asymptotic stage. For that case, the interface becomes unstable and the roll-up or pinching phenomenon appears at the final stage as we found in the previous section. On the other hand, stable oscillatory motion is possible for large surface tension coefficients. We show this stable motion in Sec. 4.2. As we see from Eq. (17), the system can be unstable when $Ag > \sigma/2$ for $g \neq 0$, where we always assume that $Ag > 0$ in our calculations. Motion of the interface for this case is shown in Sec. 4.3. When the marginally stable case that $Ag = \sigma/2$, there appears strange motion that is at rest for a long time and occurs a weak pinching phenomenon at the final stage. This critical motion for the RT instability is also described in Sec. 4.3.

4.2 Asymptotic oscillatory motion in Richtmyer-Meshkov instability

Figure 7 shows the growth rate of bubble and spike at the linear stage (up to $t = 0.5$) for various Atwood numbers. We do not use the regularized parameter δ in the calculation for $\sigma = 0$ here, therefore, the deviation from ± 1 at $t = 0$ observed in Fig. 4 does not exist in Fig. 7. Each line for $\sigma \neq 0$ represents the growth rate for all σ from $\sigma = 0.05$ to $\sigma = 1.0$ at the Atwood number which is denoted in the figure except $A = 1.0$, i.e., the growth rate does not depend on the surface tension coefficient when an Atwood number is fixed. When $A = 1.0$, slight deviations begin to appear in the growth rate of spike from the neighborhood of $t = 0.2$ for various σ. We choose $\sigma = 0.1$ for $A = 1.0$ in the figure, however, the growth rate of spike becomes smaller in its absolute value if we take larger σ. The growth rate of bubble is larger for smaller Atwood

Fig. 7: Growth rate (velocity) of bubble and spike at the linear stage, where the solid, dashed and dot-dashed lines denote $A = 0.2$, 0.5 and 1.0 with finite surface tension parameters, respectively. The solid line with circle denotes $A = 0.2$ with $\sigma = 0$.

numbers, while the growth rate of spike is larger for larger Atwood numbers (in its absolute value) regardless of the value of surface tension coefficient. This tendency is also observed for $\sigma = 0$ [13].

When we compare at the same Atwood number $A = 0.2$, the growth rate of bubble for $\sigma = 0$ is larger than the one for finite σ, while the growth rate of spike for $\sigma = 0$ is smaller than that for finite σ in its absolute value. This deviation and Eq. (16) suggest that the linear growth rate of an interface with finite σ does not obey the well-known result in the RM instability that it is proportional to time t [12, 19] at the linear stage. The calculation for $\sigma = 0$ with $\delta = 0$ breaks down at $t = 0.93$ (see Fig. 5) due to the appearance of curvature singularity, therefore, we cannot compare two lines of $\sigma = 0$ and $\sigma \neq 0$ for $\delta = 0$ up to the fully nonlinear stage such that the roll-up appears. However, the asymptotic growth rate for $\sigma = 0$ coincides with that for finite σ in the long-time computation when we use the regularized parameter δ as found in Fig. 4.

From equation (16), we see that the interface in the RM instability ($g = 0$) can oscillate with frequency $\omega = \sqrt{\sigma/2}$ for $\sigma \neq 0$. When σ is small, the inertial force exceeds the surface tension effect and concentration of vorticity arises to the roll-up of the interface. When σ is large, the surface tension stabilizes the system and as a result, a kind of periodic motion appears. Figure 8 (a) and (b) show this oscillation for $A = 0.2$ with $\sigma = 2.0$. The spike which continues to grow downward turns over at $t = 2.0$, starts to grow upward and turns over again at the neighborhood of $t = 6.0$. This oscillation is also confirmed by motion of bubble and spike in (b). The velocities of bubble and spike are equal to zero at $t = 2.0$, 5.8 and 9.5, those correspond to times at which the amplitudes of bubble and spike become maximum in their absolutes values and the turning over occurs. The maximum sheet strength κ with various surface tension coefficients is depicted in Fig. 8 (c), where we take the time step $\Delta t = 1.25 \times 10^{-4}$ for calculations of $\sigma < 1.0$ and $\Delta t = 6.25 \times 10^{-5}$ for calculations of $\sigma \geq 1.0$, respectively. As we see from the figure, the period of oscillation is longer for smaller surface tension coefficients. Time at which the maximum sheet strength κ takes the minimum value corresponds to the turning over time of bubble and spike and the time interval, i.e., the period which the minimum value appears, is almost constant when we fix a surface tension coefficient.

Every motion for $\sigma \geq 0.2$ was stable and sharp concentration in the sheet strength κ or the growth of high wave number components in the Fourier mode of the interfacial amplitude, which are signs whether the calculation breaks down or not, were not found. We add that the frequency of oscillation is little affected by the Atwood number, i.e., we obtain 'similar' motion with the same frequency for larger Atwood numbers for a fixed surface tension coefficient when it is sufficiently
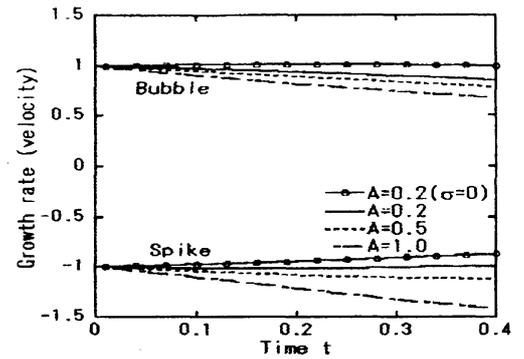
large ($\sigma \geq 0.2$), where 'similar' indicates that time at which the turning over of an interface occurs is almost the same, however, the profile of the interface or sheet strength κ is different for each Atwood number. The oscillatory motion in the RM instability is not so regular as found in the standing wave solution ($Ag < 0$) for the RT instability [20] and the frequency of oscillation is not constant even though when $A = 0$. The period of oscillation depends on the surface tension parameter and it becomes shorter as the surface tension parameter becomes larger.

4.3 Unstable and critical motion in Raighley-Taylor instability

In this subsection we present some interfacial profiles for the RT instability for the comparison with the RM instability. Initial conditions for the RT instability ($g \neq 0$) are taken that

$$x(\beta, 0) = 0, \quad y(\beta, 0) = -0.1\cos\beta, \quad \gamma(\beta, 0) = 0, \text{(18)}$$

for various g, where the gravity g is normalized as $g \rightarrow g/(kv_{lin}^2)$ with the wave number and the linear growth rate in the system [13].

Figure 9 (a) shows the temporal evolution of the interface for $A = 0.2$ with $g = 10$ and $\sigma = 1.0$, where the time step is taken that $\Delta t = 6.25 \times 10^{-5}$ and the refinement from $N = 1024$ ($0 \leq t \leq 4.0$) to $N = 2048$ ($4.0 \leq t \leq 5.0$) is performed. We see that the roll-up appears in spite of that the surface tension coefficient is sufficiently large, where the circled regions which the pinching phenomenon appears do not stick perfectly. Motion in the RM instability with the corresponding parameters excluding g is stable oscillation depicted in Fig. 8 (c) and the roll-up or the pinching phenomenon does not appear. This suggests that the gravity is effective for concentration of vorticity. The roll-up gradually disappears as the gravity g becomes small when the Atwood number and the surface tension coefficient are fixed.

Figure 9 (b) shows interfacial profiles for $A = 1.0$ with $g = 0.5$ and $\sigma = 0.5$, where the time step Δt is taken that $\Delta t = 1.25 \times 10^{-4}$ and the refinement from $N = 1024$ ($0 \leq t \leq 12.0$) to $N = 2048$ ($12.0 \leq t \leq 13.0$, $t = 13.0$ is the breakdown time here) is performed. The Atwood number $A = 1.0$ with finite g indicates that the considered system is a drop rather than a vortex sheet. The single-valuedness of the interfacial shape breaks at $t = 13.0$, however, the roll-up does not appear. Generally, the roll-up does not appear for $A = 1.0$ regardless of the value of g (including $g = 0$) or the surface tension coefficient. When we rise the value
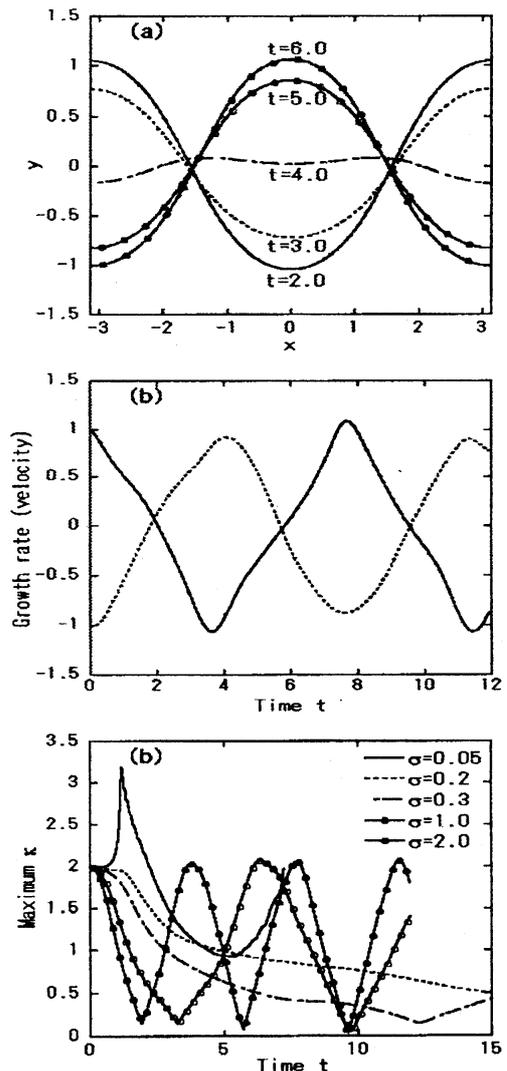

Fig. 8: Stable oscillatory motion in the RM instability for $A = 0.2$ with large σ; (a) the interfacial profiles and (b) the growth rate (velocity) of bubble and spike for $\sigma = 2.0$, where the solid and dashed lines in (b) denote bubble and spike, respectively, and (c) the maximum sheet strength κ for various surface tension coefficients ($\sigma = 0.05 - 2.0$).

of g fixing the Atwood number and the surface tension parameter, the spread into the lateral direction of the 'head' part at the final stage gradually disappears as found in the line at $t = 10.0$ in the figure, and the breakdown of computation occurs at earlier time.

The profiles presented in Fig. 9 are examples of unstable motion which satisfies $Ag > \sigma/2$ in Eq. (17). When $Ag < \sigma/2$, interfacial motion is stable oscillation and the oscillation can be regarded as a kind of standing wave which appears for $Ag < 0$. When the critical situation that $Ag = \sigma/2$, there appears motion which does not almost move for a long time and grows rapidly at the final stage. We show this critical motion in Fig. 10, where the time step is $\Delta t = 1.25 \times 10^{-4}$ and we refine $N = 512$ ($0 \le t \le 28.0$) to $N = 1024$ ($28.0 \le t \le 32.0$), and further to $N = 2048$ ($32.0 \le t \le 34.2$). The interface and the sheet strength κ (therefore, also the circulation Γ) do not change their initial shapes Eq. (18) up to the neighborhood of $t = 28.0$, and after this long linear stage, the interface grows rapidly as found in Fig. 10 (a) and (b). The maximum sheet strength κ or the growth rate of bubble and spike at the linear stage grows with some oscillation little by little as found in (c). We take parameters $A = 0.2$, $g = 5.0$ and $\sigma = 2.0$ here, however, such motion stated above appears for any parameters which satisfy the relation $Ag = \sigma/2$, although the interval of its linear stage differs by the value of g. Generally, the interval of the linear stage is longer for smaller g.

5 Discussions and conclusion

We have investigated motion of the density stratified interface with surface tension. Calculations performed here have spectral, i.e., exponential accuracy and we can regard obtained results as exact solutions of the Euler equation within machine accuracy. We presented with the accuracy that the roll up of the interface can occur for relatively small Atwood numbers without the regularized parameter δ in both of the RM and RT instabilities. We have also shown that the pinching phenomenon caused by a vortex pair induced on the interface appears for both instabilities and the gap between closest two points becomes wider as the Atwood number becomes large.

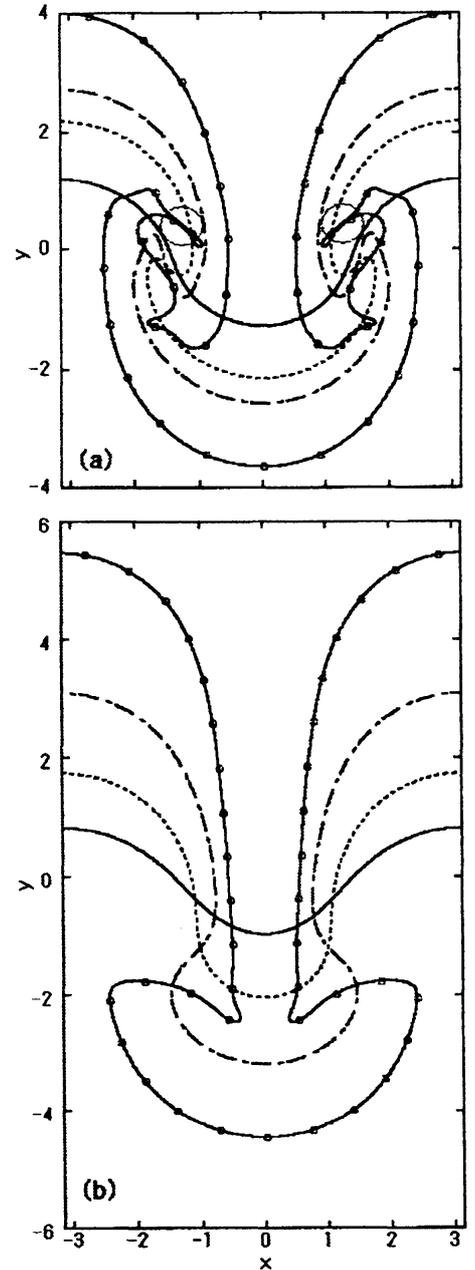For large surface tension coefficients, we have

Fig. 9: Temporal evolution of an interface in the Rayleigh-Taylor instability for (a) $A = 0.2$, $g = 10$ and $\sigma = 1.0$, and (b) $A = 1.0$, $g = 0.5$ and $\sigma = 0.5$, where the solid, dashed, dot-dashed and solid with circle lines in (a) denote $t = 2.8$, 3.6, 4.0 and 5.0, respectively, while those lines in (b) denote $t = 6.0$, 8.0, 10.0 and 13.0, respectively.

shown that there exists stable oscillatory motion for the RM instability. Such oscillatory motion is also possible for the RT instability if the relation that $Ag < \sigma/2$ is satisfied for the Atwood number A, the gravity g and the surface tension σ, however, the motion is more regular than the one for the RM instability, as found in the standing wave motion for $Ag < 0$. When $Ag = \sigma/2$, we have found marginally stable motion which needs a very long time in order to reach the nonlinear growth appears. This marginally stable motion is possible for any parameter values of the Atwood number A, the gravity g and the surface tension σ, and the length of the linear stage depends on the value of the gravity g. We mention here that the oscillatory motion in the RM instability is not linear motion and the stability of the system is determined due to the competition between the surface tension and the inertial force which effect should appear in the higher order. Detailed nonlinear analysis will be presented elsewhere.

Acknowledgments

REFERENCES

1) R.D. Richtmyer, Comm. Pure. Appl. Math. **13**, 297 (1960), E. E. Meshkov, Fluid Dyn. **4**, 101 (1969).

2) A.L. Velikovich, Phys. Fluids **8**, 1666 (1996).

3) A. Celani, A. Mazzino and L. Vozella, Phys.Rev.Lett. **96**, 134504 (2006), W. Cabot and A. W. Cook, Nature Phys. **2**, 562 (2006), M. Chertkov, Phys.Rev.Lett. **91**, 115001 (2003).

4) W. D. Arnett, J. N. Bahcall, R. P. Kirshner and S. E. Woosley, Ann. Rev. Astron. Astrophys. **27**, 629 (1989).

5) G. B. Whitham, in *linear and Nonlinear Waves*, (John Wiley & Sons, 1999).

6) H. Okamoto and M. Shoji, in *The mathematical theory of permanent progressive water-waves*, (World Scientific, 2001).

7) J. Eggers, Rev. Mod. Phys. **69** 865 (1997) [references therein].

8) T. Kadono and M. Arakawa, Icarus **173** 295 (2005).

9) J. W. Jacobs and J. M. Sheeley, Phys. Fluids **8**, 405 (1996).

10) M. A. Jones and J. W. Jacobs, Phys. Fluids **9**, 3078 (1997).

11) P. R. Chapman and J. W. Jacobs, Phys. Fluids **18**, 074101 (2006).

12) C. Matsuoka, K. Nishihara and Y. Fukuda, Phys. Rev. E **67**, 036301 (2003), **68**, 029902(E) (2003).

13) C. Matsuoka and K. Nishihara, Phys. Rev. E **73**, 026304 (2006) [references therein], **74**, 049902(E) (2006).

14) T. Y. Hou, J. S. Lowengrub and M. J. Shelley, J. Comput. Phys. **114**, 312 (1993).

15) T. Y. Hou, J. S. Lowengrub and M. J. Shelley, Phys. Fluids **9**, 1933 (1997).

16) D. Leppinen and J. R. Lister, Phys. Fluids **15**, 568 (2003).

17) D. W. Moore, Proc. Roy. Soc. London, Ser. A **365**, 105 (1979).

18) C. Matsuoka and K. Nishihara, Phys. Rev. E **73**, 055304(R) (2006).

19) C. Matsuoka and K. Nishihara, Phys. Rev. E **74**, 066303 (2006).

20) H. D. Ceniceros and T. Y. Hou, Math. Comput. **67**, 137 (1998).

21) P. G. Saffman, in *Vortex Dynamics*, (Cambridge, 1992), pp. 141.

22) G.R. Baker, D. I. Meiron and S.A. Orszag, J. Fluid Mech. **123**, 477 (1982).

23) J. T. Beale, T. Y. Hou and J. Lowengrub, SIAM J. Numer. Anal. **33**, 1797 (1996).

24) A. Sidi and M. Israeli, J. Sci. Comput. **3**, 201 (1988).

25) G. Baker and A. Nachbin, SIAM J. Sci. Comput. **19**, 1737 (1998).

26) J. G. Wouchuk and K. Nishihara, Phys. Plasmas **3**, 3761 (1996), **4**, 1028 (1997).
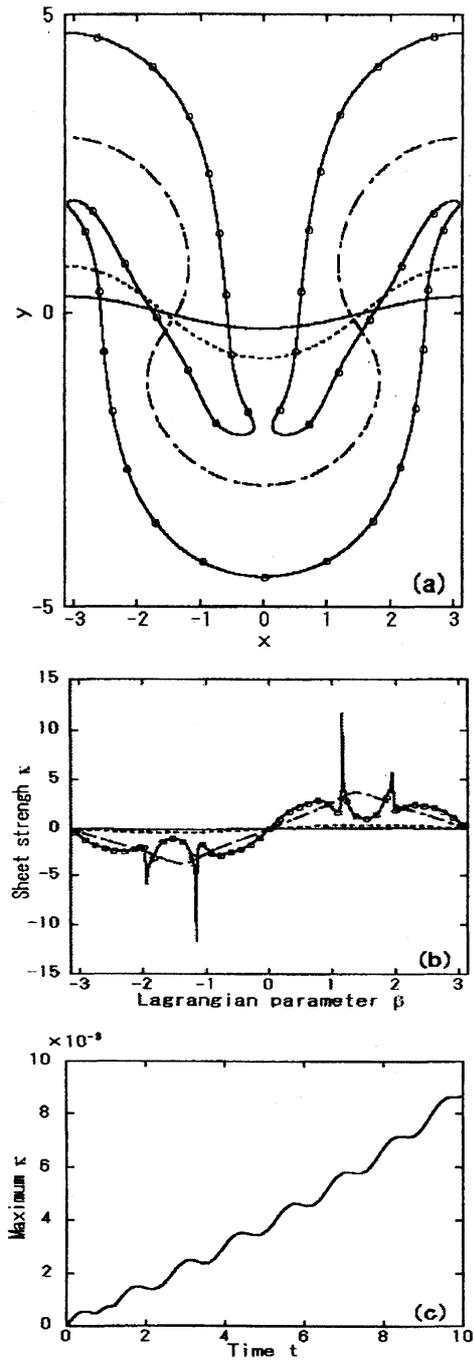
27) R. Krasny, J. Fluid Mech. **184**, 123 (1987).

Fig. 10: Temporal evolution of an interface (a), sheet strength κ (b) and the maximum sheet strength at the initial stage (c) for $A = 0.2$, $g = 5.0$ and $\sigma = 2.0$, where the solid, dashed, dot-dashed and solid with circle lines in (a) and (b) depict $t = 22.0$, 28.0, 32.0 and 34.2, respectively.